

# Manganese Ferrite Grown at the Atomic Scale

Xu Zuo, Fan Yang, R. Mafhoum, R. Karim, A. Tebano, G. Balestrino, Vincent G. Harris, and Carmine Vittoria, *Fellow, IEEE*

**Abstract**—Manganese spinel ferrite ( $\text{MnFe}_2\text{O}_4$ ) films were deposited at the atomic scale. In the depositions, laser pulses alternately impinged MnO and  $\text{Fe}_2\text{O}_3$  targets and sequentially deposited thin layers ( $\sim 5$  Å) of MnO and  $\text{Fe}_2\text{O}_3$  on MgO substrate, which is referred to as “artificial” films. The X-ray diffraction measurements showed that the artificial films were of spinel structure. Auger spectroscopy measurements showed that the chemical composition of the artificial ferrites were consistent with that of standard films deposited using a single target of  $\text{MnFe}_2\text{O}_4$ . However, extended X-ray absorption fine spectroscopy showed that the artificial growth technique affected the cation distribution to be different from the standard films. As a result, the magnetic properties of the artificial films, including Néel temperature, uniaxial and in-plane anisotropy, were different from the standard films.

**Index Terms**—Artificial film, ferromagnetic resonance, laser ablation deposition, magnetic anisotropy, spinel ferrite.

## I. INTRODUCTION

MANGANESE FERRITE ( $\text{MnFe}_2\text{O}_4$ ) is a typical partial inverse spinel ferrite [1]. In the spinel structure, the oxygen sublattice forms cation sites with tetrahedral and octahedral local symmetries, which are referred to as A and B sites, respectively [2]. In a normal spinel, the divalent cations only occupy A sites and trivalent only B sites. In an inverse spinel, the divalent cations occupy half of B sites, and trivalent cations occupy the rest A and B sites. However, due to the similarity of manganous ( $\text{Mn}^{2+}$ ) and ferric ( $\text{Fe}^{3+}$ ) cations in manganese ferrite, the cation distribution in  $\text{MnFe}_2\text{O}_4$  prepared under thermal-equilibrium depends on the growth temperature [3]. In detail, when the preparation temperature is above 900 °C, the inverse degree of manganese ferrite is about 20%, i.e., 20% of  $\text{Mn}^{2+}$  cations occupy B sites. When the preparation temperature is lower than 900 °C, the inverse degree decreases as temperature decreases [3]. As a result, the degree of inverse is limited in the range ( $<20\%$ ) by the thermo-equilibrium preparation techniques. In this research, we explored a new method to grow spinel ferrite layer-by-layer using pulsed laser ablation technique and how it impacts the magnetic properties of the films.

## II. FILM DEPOSITION

The spinel structure can be regarded as a rocksalt structure, where one face center lattice in the rocksalt structure is occu-

Manuscript received October 15, 2003. This work was supported in part by the U.S. National Science Foundation under Award DMR-0226544.

X. Zuo, F. Yang, V. G. Harris, and C. Vittoria are with the Department of Electrical and Computer Engineering, Northeastern University, Boston, MA 02115 USA (e-mail: xzuo@ece.neu.edu).

R. Mafhoum and R. Karim are with ADE Technologies, Inc., Westwood, MA 02466 USA.

A. Tebano and G. Balestrino are with the Dipartimento Ingegneria Meccanica, Università degli Studi di Roma “Tor Vergata,” 00173 Rome, Italy.

Digital Object Identifier 10.1109/TMAG.2004.830447

TABLE I  
LATTICE CONSTANT, DEGREE OF INVERSE AND MAGNETIC PROPERTIES OF FILMS

	Artificial (111)	Artificial (100)	Standard (111)	Standard (100)
$a$ (Å) <sup>(a)</sup>	8.51	8.53	8.51	8.53
$x$ <sup>(b)</sup>	0.64	0.66	0.51	0.42
$T_N$ (°K)	523	512	583	585
$4\pi M_S^{RT}$ (kG)	2.6	2.0	3.0	2.5
$H_u$ (kOe) <sup>(c)</sup>	0.16	2.40	0.20	0.50
$\Delta H$ (Oe)	40	400	200	260

(a) Since  $\theta$ - $2\theta$  scans were performed in XRD measurement, the lattice constant measured for (100) film were the distance between two neighbor

(100) planes. When there is tetragonal distortion along [100] direction, this value corresponds to  $c$ .

(b) We write the general chemical formula of manganese ferrite as  $\text{Mn}_{1-x}\text{Fe}_x[\text{Mn}_x\text{Fe}_{2-x}]\text{O}_4$ , where “[ ]” means on B sites.

(c)  $H_u$  measured in (111) films corresponds to the cubic anisotropy field  $-2K_1/M_s$ .

ried by A site clusters containing 2 A site cations and 4 oxygen anions ( $\text{O}^{2-}$ ) and the other by B site clusters containing 4 B site cations and 4  $\text{O}^{2-}$  anions [4]. In this picture, the spinel structure can be regarded as a layer-by-layer packing of planes containing only A or B site clusters along the  $\langle 111 \rangle$  direction.

Following the above picture, we used two targets, manganese monoxide (MnO) and iron oxide ( $\text{Fe}_2\text{O}_3$ ) in the pulsed laser ablation deposition of  $\text{MnFe}_2\text{O}_4$ . The two targets were mounted on a revolver-like target rotator, which was synchronized with the trigger of the laser. The laser was tuned to a power of 400 mJ per pulse (typical duration of 50 ns) and a repeat rate of 2 Hz. The numbers of pulses shot on MnO and  $\text{Fe}_2\text{O}_3$  targets in each cycle were set to 4 and 8, respectively. The combination of laser energy and numbers of pulses on targets in a cycle was determined by separated depositions of MnO and  $\text{Fe}_2\text{O}_3$ , in order to ensure that the mole ratio of manganese to iron was 1 : 2 and that the amount of MnO (or  $\text{Fe}_2\text{O}_3$ ) corresponded to a single layer of A (or B) site clusters. In each deposition, we ran 1000 cycles, which lasted about 4 h in time. In the deposition, the chamber was flushed by oxygen ( $\text{O}_2$ ) gas mixture at 50 mtorr. To grow  $\text{MnFe}_2\text{O}_4$  epitaxially, we chose magnesium oxide (MgO) single crystal substrates, both  $\{111\}$  and  $\{100\}$  planes. The lattice constant of MgO is 4.2112 Å [5], which is about one half of  $\text{MnFe}_2\text{O}_4$  ( $a = 8.511$  Å [6]). The substrates were mounted on a substrate holder and heated at 700 °C.

The films deposited by above procedure are referred to as “artificial.” For comparison purpose, we also deposited

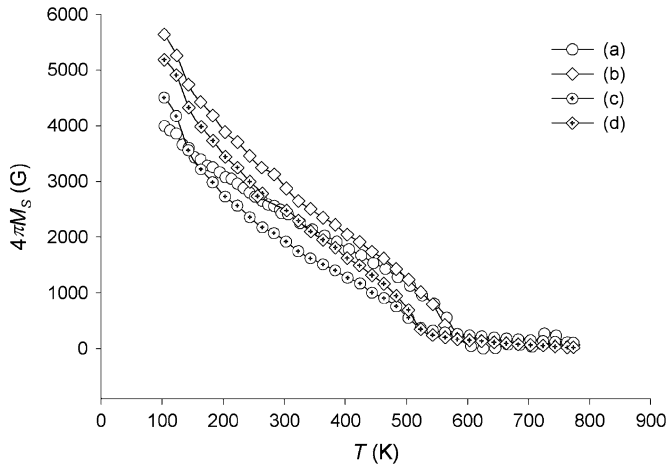


Fig. 1. Magnetization versus temperature of (a) standard {100} film, (b) standard {111} film, (c) artificial {100} film, and (d) artificial {111} film.

$\text{MnFe}_2\text{O}_4$  from a single  $\text{MnFe}_2\text{O}_4$  target on the same substrates under the same conditions. The films were referred to as “standard” films.

### III. MAGNETIC PROPERTIES

The crystal structure of both artificial and standard films was determined to be spinel by X-ray diffraction (XRD). XRD indicated that the films were epitaxially grown on the substrates. The measured lattice constants are listed in Table I. The Auger spectroscopy measurements of both artificial and standard films confirmed that the manganese to iron ratio was about 1 : 2. These results implied that the artificial films were almost identical to the standard ones in the sense of crystal structure and chemical composition. However, the extended X-ray absorption fine spectroscopy (EXAFS) [7] measured that the cation distribution of artificial films was different from the standard ones. EXAFS measured a larger degree of inverse ( $x$ ) in artificial films than standard films (Table I). The details and results of EXAFS measurements are reported independently in another paper. In this paper, we focus on the impacts of the artificial growth technique on the magnetic properties of the films.

The Néel temperatures of artificial and standard films were measured by measuring the magnetic moment as a function of temperature (Fig. 1). The Néel temperature of artificial film was 60–70 K smaller than the standard film deposited on the same plane (Table I). At room temperature ( $\sim 293$  K), the saturation magnetization ( $4\pi M_S$ ) of artificial films was 0.4–0.5 kG smaller than the standard film deposited on the same plane, and  $4\pi M_S$  of {100} films was 0.5–0.6 kG smaller than {111} films (Table I).

The magnetic uniaxial anisotropy fields ( $H_u$ ) in the films were measured by ferromagnetic resonance (FMR) technique (Table I) using a center mounted  $\text{TE}_{102}$  rectangular resonator at X-band. In the measurement, the external magnetic field was perpendicular to the film plane and the FMR frequency can be written as

$$f/\gamma' = H_{\text{ext}} - 4\pi M_S + H_u \quad (1)$$

where we assume  $\gamma' = 2.8$  GHz/kOe corresponding to  $g = 2.0$  [8]. From FMR measurement,  $H_u$  was measured to be 2.4 kOe

in artificial {100} film and 0.5 kOe in standard {100} film. Small  $H_u$  was measured by FMR in artificial and standard {111} films as 0.16 and 0.20 kOe, respectively. In the FMR measurements, the FMR linewidth ( $\Delta H$ ) of the films were also measured for {100} and {111} films (Table I).

The in-plane magnetic anisotropy was also measured by FMR at Q-band for the artificial {100} film. Since  $H_u$  in the artificial {100} film is much larger than the cubic magnetic anisotropy field ( $2|K_1|/M_S \sim 180$  Oe) measured in bulk  $\text{MnFe}_2\text{O}_4$  sample [8], we derived the FMR frequency from the free energy with a tetragonal symmetry [9], which is equivalent to adding the uniaxial anisotropy energy term to cubic anisotropy in free energy. We obtain

$$\begin{aligned} f/\gamma' = & [H_{\text{ext}} \cos(\phi - \phi_H) - H_\phi \cos 4\phi]/4]^{1/2} \\ & \times [H_{\text{ext}} \cos(\phi - \phi_H) + 4\pi M_S \\ & - H_u - H_\phi(3 + \cos 4\phi)/4]^{1/2} \end{aligned} \quad (2)$$

where  $\phi_H$  is the azimuthal angle of the external magnetic field and  $\phi$  is the azimuthal angle of the static magnetization, which can be determined from

$$1/4H_\phi \sin 4\phi = H_{\text{ext}} \sin(\phi - \phi_H) \quad (3)$$

Here,  $H_\phi$  is the in-plane magnetic anisotropy field defined by

$$H_\phi = 4K_3/M_S \quad (4)$$

where  $K_3$  is the in-plane anisotropy constant in the free energy. At  $\phi_H = 0^\circ$  and  $45^\circ$ , the solution of (3) is simply  $\phi = \phi_H$ . If we assume  $H_\phi$  is small, we can approximately deduce  $H_\phi$  from  $\Delta = H_{\phi=45^\circ} - H_{\phi=0^\circ}$  as

$$H_\phi = -\Delta \frac{2H_{\text{avg}} + 4\pi M_S - H_u}{5/2H_{\text{avg}} + 8\pi M_S - 2H_u} \quad (5)$$

where  $H_{\text{avg}}$  is the average resonance field defined by

$$H_{\text{avg}} = \frac{1}{2}(H_{\phi=0^\circ} + H_{\phi=45^\circ}). \quad (6)$$

In Fig. 2, we plot the resonance field ( $\Delta H_R$ ) after the deduction of zero order ( $H_{\text{avg}}$ ) and second-order harmonics as a function of  $\phi_H$  and observe a fourfold symmetry. We deduced  $H_\phi = 350$  Oe in artificial {100} film.

### IV. DISCUSSION AND CONCLUSION

In Table I, we summarized structural and magnetic properties of the studied layers. We found significant differences in  $H_u$  value among the films. Small  $H_u$  were observed in {111} films, while large  $H_u$  in artificial {100} films. From the magnitude of  $H_u$ , we may conclude that  $H_u$  in {111} films may correspond to cubic magnetic anisotropy field  $-2K_1/M_S$  [8]. For the same reason, we have excluded that  $H_u$  in {100} films originated from cubic anisotropy. We may attribute the large  $H_u$  in {100} films to two major contributions, the magnetostriction and cooperative Jahn–Teller effect.

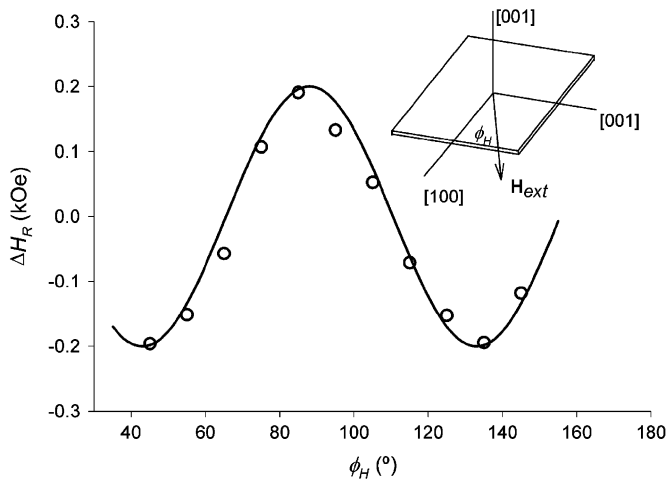


Fig. 2. The fourfold symmetry pattern of in-plane FMR of artificial {100} film.

For an isotropic stress ( $\sigma$ ) on {100} substrate, the uniaxial anisotropy energy term added to cubic anisotropy can be written as [10]

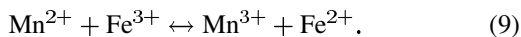
$$F_s = -(3\sigma/2)\lambda_{100} \cos^2\theta \quad (7)$$

where  $\lambda_{100}$  is the magnetostriction coefficient along {100} direction. From (7),  $H_u$  can be written as

$$H_u = 3\sigma\lambda_{100}/M_S. \quad (8)$$

Using  $\lambda_{100} = -25 \times 10^{-6}$  measured for bulk  $\text{MnFe}_2\text{O}_4$ , we deduced  $\sigma = -5.47 \times 10^9$  and  $-1.80 \times 10^9$  dyne/cm<sup>2</sup> for artificial and standard {100} films, respectively, where we subtract the cubic anisotropy contribution  $2K_1/M_S \sim -180$  Oe. If we assume that the isotropic stress does not affect the cubic anisotropy in the free energy, we can deduce  $K_3 = -K_1/2$ , where  $K_1$  is the cubic anisotropy. Thus, from measured  $H_\phi$ , we deduce  $2K_1/M_S = -350$  Oe, which is about two times the value measured for bulk  $\text{MnFe}_2\text{O}_4$  and {111} films. Also, we find that the large  $H_u$  in {100} films are correlated with large  $\Delta H$  (Table I), which implies an anisotropy mechanism correlated with magnetic loss. Above observations lead us to the possible Jahn–Teller effects.

In  $\text{MnFe}_2\text{O}_4$ , the active cation of Jahn–Teller effect is  $\text{Mn}^{3+}$  coming from electrons can transfer by the process on B sites [11]



From previous research on conductivity [11], the activation energy of the process (9) was 0.3 eV for stoichiometry bulk sample, which corresponds to very low concentration of  $\text{Mn}^{3+}$  at room temperature. In this case, local Jahn–Teller effect of  $\text{Mn}^{3+}$  tetragonally distorts the octahedrals with  $c/a > 1$  and the thermo-energy randomly orient the tetragonal axis along

$\langle 100 \rangle$  directions. The local Jahn–Teller effect does not raise macroscopic anisotropy due to the random orientation of the distorted octahedrals, although the large  $D$  coefficient in the spin Hamiltonian [12] of  $\text{Mn}^{3+}$  in tetragonal symmetry implies large single ion anisotropy. It, however, does raise an additional magnetic loss mechanism contributing to  $\Delta H$ , since it directly couples spins to phonons [13].

When the concentration of  $\text{Mn}^{3+}$  is high enough [14] or there is a uniaxial stress field along one of  $\langle 100 \rangle$  directions strong enough, the equilibrium of (9) moves toward the right-hand side and the tetragonal axis of distorted octahedrals aligned along one of  $\langle 100 \rangle$  directions of the uniaxial stress field, which is referred to as cooperative Jahn–Teller effect [15]. In such a case, the cooperative Jahn–Teller effect raises a tetragonal distortion of the cubic unit cell and macroscopic magnetic anisotropy from the large single ion anisotropy of  $\text{Mn}^{3+}$ .

In {100} films, the degree of inverse ( $x$ ) plays an important role, since the cooperative Jahn–Teller effect indirectly depends concentration of  $\text{Mn}^{2+}$  on the left-hand side of (9). From chemical equilibrium, a higher concentration of  $\text{Mn}^{2+}$  on the left-hand side of (9) leads to higher concentration of  $\text{Mn}^{3+}$ , which implies larger uniaxial magnetic anisotropy and magnetic loss that can be qualitatively confirmed by measured  $H_u$  and  $\Delta H$  in Table I.

## REFERENCES

- [1] J. M. Hastings and L. M. Corliss, "Neutron diffraction study of manganese ferrite," *Phys. Rev.*, vol. 104, pp. 328–331, 1956.
- [2] E. W. Gorter, "Saturation magnetization and crystal chemistry of ferrimagnetic oxides," *Philips Res. Rep.*, vol. 9, pp. 295–320, 1954.
- [3] S. Krupička and P. Novák, "Oxide spinel," in *Ferromagnetic Materials*, E. P. Wohlfarth, Ed. Amsterdam, The Netherlands: North-Holland, 1982, vol. 3, p. 209.
- [4] J. Smit and H. P. J. Wijn, *Ferrites*. New York: Wiley, 1959, p. 137.
- [5] R. W. G. Wyckoff, *Crystal Structure*, 2nd ed. New York: Interscience, 1963, vol. 1, p. 88.
- [6] R. W. G. Wyckoff, *Crystal Structure*, 2nd ed. New York: Interscience, 1965, vol. 3, p. 79.
- [7] S. Calvin, E. E. Carpenter, V. G. Harris, and S. A. Morrison, "Use of multiple-edge refinement of extended x-ray absorption fine structure to determine site occupancy in mixed ferrite nanoparticles," *Appl. Phys. Lett.*, vol. 81, p. 3828, 2002.
- [8] R. Vautier and M. Paulus, "Mn-Fe<sup>3+</sup> spinels (Mn ferrites) and Mn-Fe<sup>3+</sup> spinels with substitutions," in *Landolt-Börnstein Numerical Data and Functional Relationship*, K.-H. Hellwege and A. M. Hellwege, Eds. Berlin, Germany: Springer-Verlag, 1970, pt. b, vol. 4, pp. 160–164.
- [9] S. Krupička and P. Novák, "Oxide spinel," in *Ferromagnetic Materials*, E. P. Wohlfarth, Ed. Amsterdam, The Netherlands: North-Holland, 1982, vol. 3, p. 233.
- [10] C. Vittoria, H. Lessoff, and N. D. Wilsey, "Induced in-plane magnetic anisotropy in YIG films," *IEEE Trans. Magn.*, vol. 8, pp. 273–275, 1972.
- [11] F. K. Lotgering, "Semiconduction and cation valencies in manganese ferrite," *J. Phys. Chem. Solids*, vol. 25, pp. 95–103, 1964.
- [12] R. Gerber and G. Elbinger, "Contribution of Fe<sup>2+</sup>, Mn<sup>3+</sup>, and Fe<sup>3+</sup> ions to the anisotropy of Mg<sub>x</sub>Mn<sub>0.6</sub>Fe<sub>2.4-x</sub>O<sub>4</sub>," *J. Phys. C*, vol. 3, pp. 1363–1375, 1970.
- [13] S. Krupička and K. Závěta, "Magnetic aftereffects in ferrimagnetic oxidic spinels," *J. Appl. Phys.*, vol. 39, pp. 930–938, 1968.
- [14] V. A. M. Brabers, "Cation migration, cation valencies and the cubic-tetragonal transition in Mn<sub>x</sub>Fe<sub>3-x</sub>O<sub>4</sub>," *J. Phys. Chem. Solids*, vol. 32, pp. 2181–2191, 1971.
- [15] G. A. Gehring and K. A. Gehring, "Co-operative Jahn–Teller effects," *Rep. Prog. Phys.*, vol. 38, pp. 1–89, 1975.